On the Limits of State-of-the-Art GNSS Receivers in Frequency Transfer

Thomas Krawinkel and Steffen Schön

Abstract

GNSS frequency transfer (FT) based on precise point positioning delivers instability values down to sub-10^{-16} between two modern receivers. In the present study we investigate the technical limits such receivers impose on FT by means of a dedicated experiment at Germany's national metrology institute (PTB). For this purpose, four geodetic receivers, two of the same type each, were all connected to one single antenna and fed by the highly stable UTC (PTB) frequency signal. Since all error sources affecting the satellite signals are the same for all receivers, they cancel out when forming receiver-to-receiver single differences (SDs). Due to the fact that the remaining SD carrier phase ambiguities can be easily fixed to integer values, only the relative receiver clock error remains in the SDs. We assess the instability of three different receiver combinations, two with the same receiver type (intra-receiver) and one with different types (inter-receiver). The intra-receiver pairs reach lower instability values faster than the inter-receiver combination, which is in part caused by the different signal tracking modes of the receivers. To be specific, the 10^{-18} instability range was only reached by the intra-receiver pairs, whereas the inter-receiver combination already hits its noise floor at about $1.5 \cdot 10^{-17}$. In addition, our analysis of using different observation type combinations only shows small differences regarding the link instability.

Keywords

Allan deviation · Frequency transfer · GNSS

1 Introduction

Today, frequency transfer (FT) based on Global Navigation Satellite System (GNSS) measurements is used as a standard technique (Defraigne 2017). To this end, GNSS receivers are connected to frequency standards or atomic clocks whose frequency is to be compared. Typically, the recorded GNSS data are analyzed using the precise point positioning (PPP) method (Zumberge et al. 1997). The obtained receiver clock error time series of different stations serve as a starting quantity for frequency transfer. Currently, on the analysis side, GNSS FT achieves sub-10^{-16} instability values by means of integer PPP (Petit 2021). On the side of the receivers, the stability of the internal hardware delays is most important for the achievable FT instability. This includes delay variations in each receiver itself as well as different behaviors of these variations between the receivers involved. In theory, if all error sources were eliminated or well controlled, the instability of GNSS-based FT should be dominated by white frequency noise at the level of the noise of the GNSS

This research was funded by the Deutsche Forschungsgemeinschaft (DFG, German Research Foundation) – project number 434617780 – SFB 1464.

T. Krawinkel (✉) · S. Schön
Leibniz University Hannover, Institut für Erdmessung, Hannover, Germany
e-mail: krawinkel@ife.uni-hannover.de

J. T. Freymueller, L. Sánchez (eds.), *Geodesy for a Sustainable Earth*,
International Association of Geodesy Symposia 154, https://doi.org/10.1007/1345_2022_145

observation type in use. When using modern, state-of-the-art GNSS receivers, this limit would be in the range of a few millimeters. According to manufacturer's data, for example JAVAD GNSS (2021), carrier phase precision – in zenith direction – amounts to 1 mm. In order to also take into account noisier GNSS observations in low elevation angles, we assess the range limit to 1–3 mm.

On our way to pushing the limits of GNSS FT to the instability range of 10^{-17} within the framework of the Collaborative Research Centre *TerraQ (Relativistic and Quantum-based Geodesy)*, in a first step, we want to assess the minimum achievable frequency instability between two GNSS receivers. The metrological foundation for our investigations is a dedicated experiment we carried out at the Physikalisch-Technische Bundesanstalt (PTB), Germany's national metrology institute, where we have the possibility to set up the receivers in a controlled environment. This means that all receivers were connected to the same antenna as well as the same frequency signal of the locally generated approximation of Coordinated Universal Time (UTC), referred to as UTC(PTB) (Bauch et al. 2012). We analyze the recorded GPS and Galileo carrier phase observations based on between-receiver single differences (SDs) with our in-house GNSS software, and examine the instability of each receiver link by means of the modified Allan deviation (Allan 1987; Allan and Barnes 1981). The remainder of the paper is structured as follows. In Sect. 2 the experimental set up is described. Next, Sect. 3 details the data analysis, and the obtained results are presented and discussed in Sect. 4.

2 Experiment

The entire GNSS measurement campaign was carried out from April 20 to May 10, 2021 in and on top of the Meitner building at PTB. Here, the receivers were installed in a laboratory where temperature and humidity were controlled by an air conditioning system. The relative humidity was steered around a value of 50% with a 1σ of 4%, and the temperature was stabilized at about 22.9 °C with a 1σ of 0.1 °C.

The main measurement equipment consisted of four modern geodetic GNSS receivers, namely two JAVAD OMEGA (serial no.: 0046, 0047) and two Septentrio PolaRx5TR (serial no.: 1345, 1372). In the first part of the experiment, which lasted for ten days (April 20–29, 2021) and which we will discuss in this article, all of these receivers were connected to one single antenna, a Leica AR20 with radome, via an active signal splitter. Furthermore, all receivers were driven by the same 10 MHz UTC(PTB) signal. Such a measurement configuration is usually referred to as a zero baseline (ZB), common clock (CC) configuration. Photographs of the installations and a schematic depiction of the measurement configuration are shown in Figs. 1 and 2.

(a) (b)

Fig. 1 GNSS equipment used during the experiment. Note that in the first part of the measurement campaign, the receivers were only connected to the left antenna. (**a**) Receivers. (**b**) Antennas

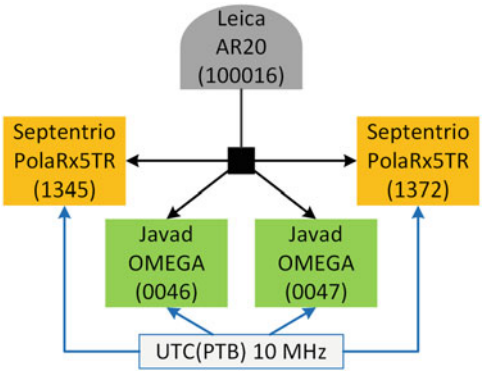

Fig. 2 Schematic depiction of the zero-baseline, common-clock measurement configuration during the experiment

The signal paths from the antenna to each receiver were identical to ensure identical delays. In addition to GPS and Galileo, the receivers track also GLONASS and BeiDou signals with a data rate of 1 Hz. A more detailed description of the experiment can be found in Krawinkel et al. (2021).

3 Data Analysis

We investigate the current technical limits of GNSS FT by means of the continuous ZB-CC measurements which lasted for ten full days as discussed in Sect. 2. To be more specific, we use our in-house MATLAB-based GNSS toolbox to analyze the GPS and Galileo carrier phase observations with a sampling interval of 30 s. In order to be able to use GPS and Galileo observations in a consistent way, we apply final satellite orbit and clock products computed within the frame of the Multi-GNSS Experiment (MGEX) project by the Centre National d'Etudes Spatiales, Collecte Localisation Satellites (CNES/CLS) (Montenbruck et al. 2017; Loyer et al. 2012; Katsigianni et al. 2019).

When forming carrier phase single differences ΔL of any signal frequency (L1, L2, etc.) in a ZB-CC measurement configuration between two receivers A, B and satellite j,

distance-dependent signal errors like atmospheric propagation delays, site-specific errors such as multipath or antenna-related cancel out. Consequently, they are not modeled or corrected in our analysis. The relative geometry can be computed from very accurate a-priori satellite and receiver coordinates. Thus, only the carrier phase ambiguity ΔN of each satellite and the relative clock offset $\Delta\delta t_{A,B}$ between the receivers remain as unknowns:

$$\Delta L^{j}_{A,B} = c \cdot \Delta\delta t_{A,B} + \lambda \cdot \Delta N^{j}_{A,B} + \Delta\epsilon_{A,B} \qquad (1)$$

with the speed of light c, carrier phase wavelength λ, and carrier phase observation noise $\Delta\epsilon_{A,B}$. Due to the fact that the observation geometries for both receivers are virtually the same, ambiguity resolution is a relatively simple task and can be achieved by means of rounding to the nearest integer value. In our case, all ambiguities could be successfully fixed to integer cycles given that the initial real-valued ambiguities were close to integer cycles by 1.5% or less.

From the ambiguity-fixed original single-frequency SD observations, we compute dual-frequency ionosphere-free (IF) observables for each receiver. Although they are noisier by a factor of three compared to single-frequency observables, we use IF observables since that is the primary observation type used in practical GNSS FT (Defraigne 2017; Weinbach 2013). Thus, we can derive more consistent and meaningful conclusions from the results – computed with IF observables – because they represent a typical GNSS FT use case.

Averaging the resulting IF SD observables of all satellites then yields one estimate for the relative receiver clock error at each measurement epoch (Weinbach et al. 2009). Finally, we do not apply any elevation-dependent weighting scheme since this slightly increases the noise of the resulting clock error time series. This behavior is visible in the two mean SD time series of the JAVAD receiver pair on the first day of the experiment shown in Fig. 3. One time series is computed with an identity weighting and the other with a cosine weighting based on the satellite elevation angle. In the end, the results when using either one of the two weighting schemes are only marginally different. Potentially erroneous observations at low elevations are eliminated by applying an elevation cutoff angle of 15°.

From the total of four receivers, we compute the results for different receiver pairs. We will discuss those of the following combinations:

1. Both JAVAD receivers
2. Both Septentrio receivers
3. One JAVAD (0046), one Septentrio (1345) receiver

Since the first two combinations use identical receivers of the same manufacturer, we refer to them as *intra-receiver* combinations, whereas the third pair is designated as an *inter-receiver* combination.

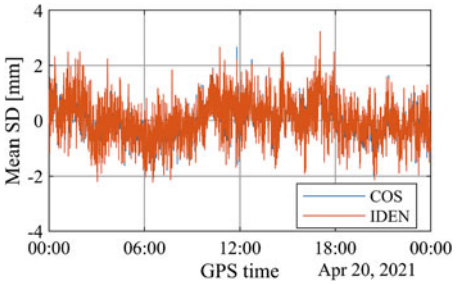

Fig. 3 Mean single differences (SDs) between the two JAVAD receivers (0046, 0047) with identity (IDEN) and cosine elevation (COS) weighting for ionosphere-free linear combination GL1C-GL2W (cf. Table 1)

4 Results

The relative receiver clock errors are represented by the mean SD of all satellites, thus we refer to the time series shown in Figs. 4, 5, 6 as such. They are computed for five different IF linear combinations based on these original observation types:

- GPS
  - L1 C/A, L2W
  - L1 C/A, L2C
  - L1 C/A, L5
- Galileo
  - E1, E5a
  - E1, E5 (AltBOC)

Because JAVAD and Septentrio receivers track GPS L2C, L5 as well as Galileo E5 signals in different ways, the designation of their respective IF combinations becomes a bit cumbersome. A description of the corresponding abbreviations used in the figures in this section can be found in Table 1.

The mean SDs for the two intra-receiver combinations and the inter-receiver pair are shown in Figs. 4, 5, 6, respectively. Since the noise of GNSS carrier phase observations is typically specified in millimeters, we choose this unit for these figures. All depicted time series are each reduced by an offset. Due to the fact that the receivers are not calibrated for any signal delays, these offsets basically represent arbitrary

Table 1 Carrier phase observation types used for ionosphere-free linear combinations in data analysis according to Romero (2020)

Abbreviation	System	Frequency (channel)
GL1C	GPS	L1 (C/A)
GL2W	GPS	L2 (Z-tracking and similar)
GL2X, GL2L	GPS	L2C (M+L), L2C (L)
GL5X, GL5Q	GPS	L5 (I+Q), L5 (Q)
EL1X, EL1C	Galileo	E1 (OS data+pilot), E1 (OS pilot)
EL5X, EL5Q	Galileo	E5a (I+Q), E5a (Q)
EL8X, EL8Q	Galileo	E5 (I+Q), E5 (Q)

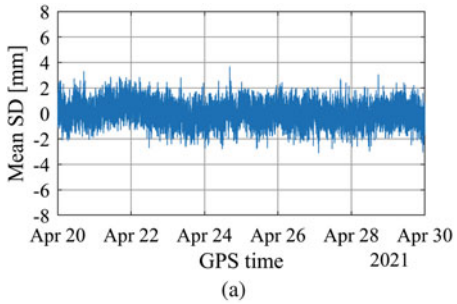

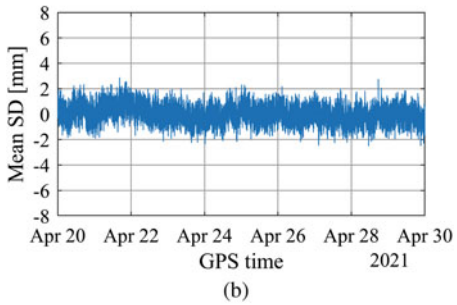

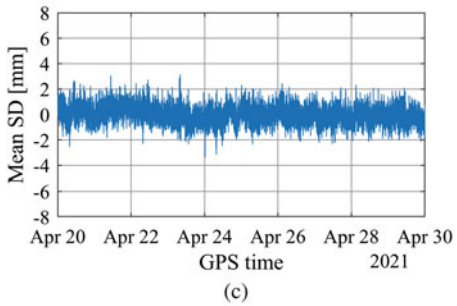

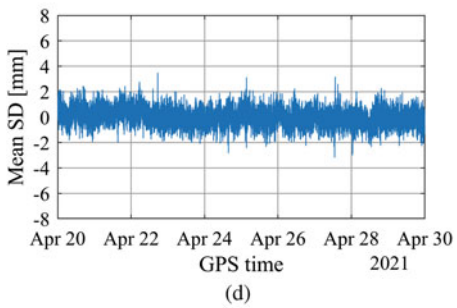

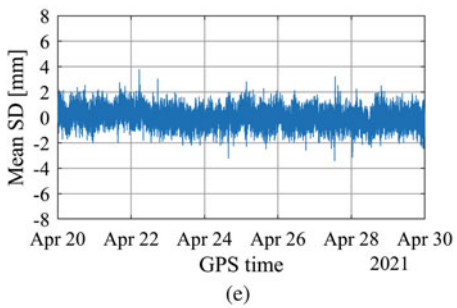

Fig. 4 Mean single differences (SDs) between the two JAVAD receivers (0046, 0047) for ionosphere-free linear combinations of various observation types. The abbreviations of the latter are explained in Table 1. (**a**) GL1C-GL2W. (**b**) GL1C-GL2X. (**c**) GL1C-GL5X. (**d**) EL1X-EL5X. (**e**) EL1X-EL8X

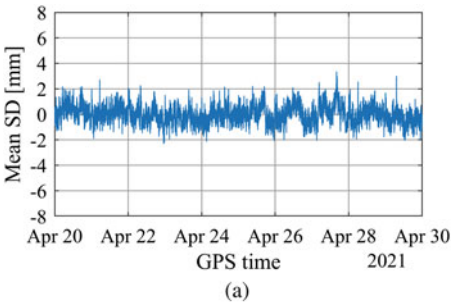

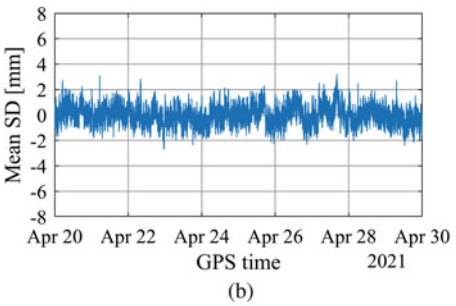

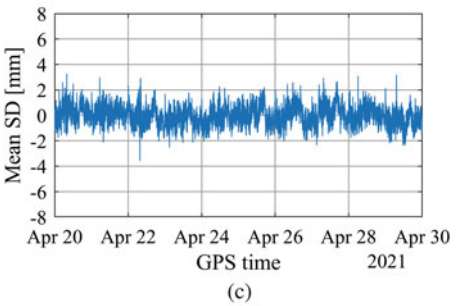

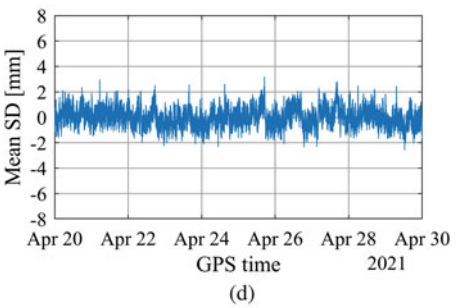

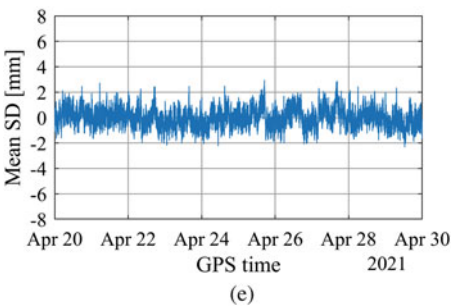

Fig. 5 Mean single differences (SDs) between the two Septentrio receivers (1345, 1372) for ionosphere-free linear combinations of various observation types. The abbreviations of the latter are explained in Table 1. (**a**) GL1C-GL2W. (**b**) GL1C-GL2L. (**c**) GL1C-GL5Q. (**d**) EL1C-EL5Q. (**e**) EL1C-EL8Q

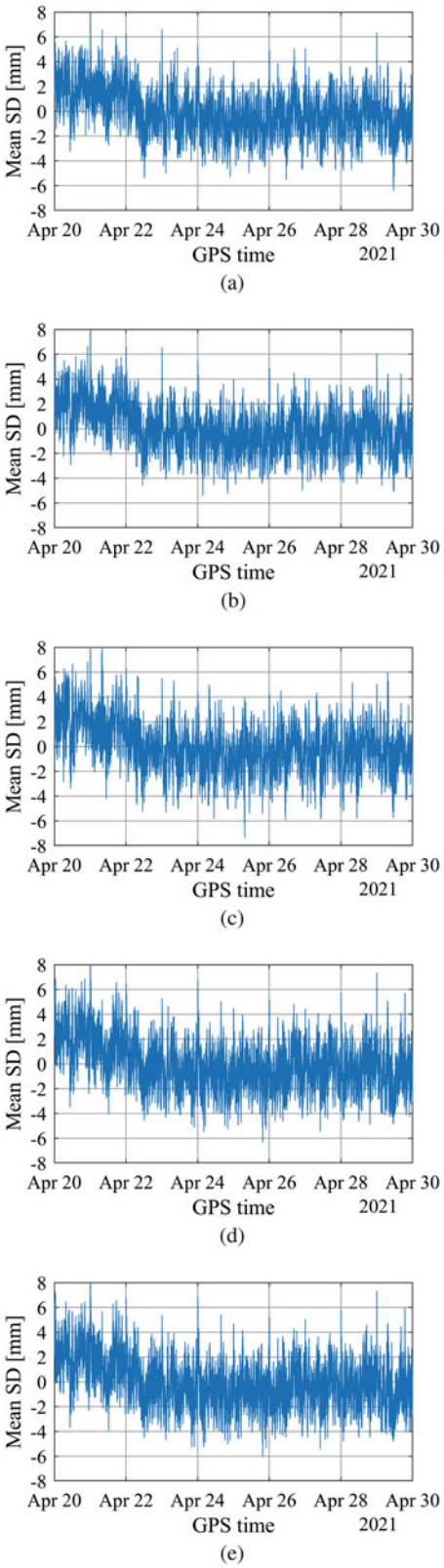

Fig. 6 Mean single differences (SDs) between the first JAVAD receiver (0046) and the first Septentrio receiver (1345) for ionosphere-free linear combinations of various observation types. The abbreviations of the latter are explained in Table 1. (**a**) GL1C-GL2W. (**b**) GL1C-GL2(X/L). (**c**) GL1C-GL5(X/Q). (**d**) EL1(X/C)-EL8(X/Q). (**e**) EL1(X/C)-EL8(X/Q)

observation-specific hardware delays between the involved receivers.

In an ideal case, the remaining time series should resemble a white noise process. From our results, the JAVAD receiver pair gets the closest to that expected behavior (Fig. 4). The time series of the Septentrio receiver combination look similar (Fig. 5). Although being less noisy in comparison, they reveal certain systematic effects. Overall, the two intra-receiver pairs have 1σ-precision levels of 0.7 mm, whereas the inter-receiver combination (Fig. 6) shows a more than two times higher value of 1.8 mm.

Furthermore, these time series also exhibit a running-in effect over the course of the first two days of the measurement campaign. Nevertheless, all these noise levels are well in the range of the assumed precision of IF carrier phase observations from a geodetic receiver of about 1–3 mm. A summary of the time series statistics, i.e. their mean values and standard deviations, is given in Table 2. Regarding the different observation types for each receiver combination, only small differences are visible.

From the mean SD results, we can derive the frequency instability of each receiver link as shown in Fig. 7 in terms of modified Allan deviations:

$$\sigma_y^2(\tau) = \frac{1}{2m^2\tau^2(N-3m+1)} \sum_{j=1}^{N-3m+1} \left(\sum_{i=j}^{j+m-1} (x_{i+2m} - 2x_{i+m} + x_i) \right)^2, \quad (2)$$

with time error measurement x_i, averaging time $\tau = m\tau_0$ consisting of averaging factor m and basic sampling interval τ_0 of a finite data set of length N.

Table 2 Mean value and standard deviation (STD) of various mean ionosphere-free single difference time series. The observation types are explained in Table 1

Receiver pair	Observation types	Mean (mm)	STD (mm)
2 JAVAD (0046, 0047)	GL1C-GL2W	56.8	0.8
	GL1C-GL2X	56.3	0.7
	GL1C-GL5X	−91.6	0.7
	EL1X-EL5X	−92.1	0.6
	EL1X-EL8X	83.9	0.7
2 Septentrio (1345, 1372)	GL1C-GL2W	245.6	0.7
	GL1C-GL2L	245.7	0.7
	GL1C-GL5Q	−15.7	0.7
	EL1C-EL5Q	−15.4	0.7
	EL1C-EL8Q	−0.7	0.7
1 JAVAD (0046), 1 Septentrio (1345)	GL1C-GL2W	−224.0	1.7
	GL1C-GL2(X/L)	−222.9	1.7
	GL1C-GL5(X/Q)	−126.5	1.8
	EL1(X/C)-EL5(X/Q)	−128.0	1.8
	EL1(X/C)-EL8(X/Q)	−174.2	1.8

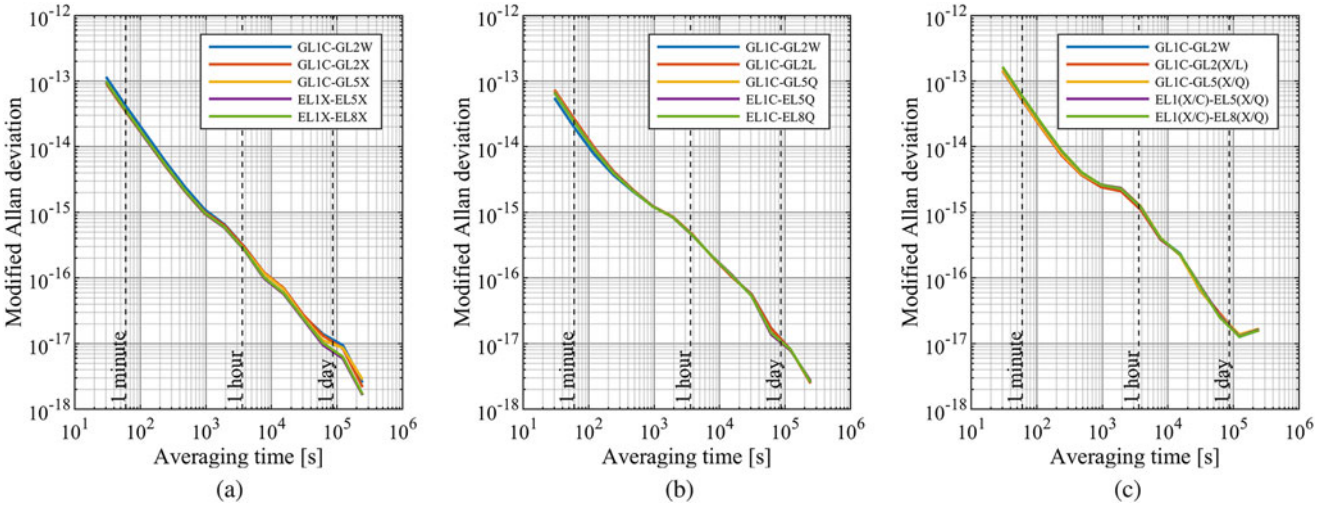

Fig. 7 Frequency instability of 10-day continuous GNSS measurements in terms of modified Allan deviations for all three receiver links for ionosphere-free linear combinations of various observation types. The abbreviations of the latter are explained in Table 1. (**a**) JAVAD (0046, 0047). (**b**) Septentrio (1345, 1372). (**c**) JAVAD (0046), Septentrio (1345)

The intra-receiver combinations provide a better overall performance than the inter-receiver pair, where the latter seems to reach its flicker floor before getting to the 10^{-18} instability range. One reason for this behavior could be that the JAVAD and Septentrio receivers use different tracking modes for modern GNSS signals. The JAVAD receiver combination reaches a frequency instability of $1 \cdot 10^{-17}$ after an averaging time of approximately 5900 s using Galileo E1-E5a (EL1X-EL5X) signals. The use of modern GPS L2C (GL2X/L) and L5 (GL5X/Q) signals results in smaller instability values as compared to legacy L1 (GL1C) and L2 (GL2W) signals. For both intra-receiver pairs, the noise floor is not yet visible in this 10-day data set.

5 Conclusions

In this contribution, we presented the results of the first part of a dedicated GNSS measurement campaign that lasted for ten days and was carried out at Germany's national metrology institute (PTB) in the spring of 2021. Four geodetic receivers, namely two JAVAD OMEGA, and two Septentrio PolaRx5TR, were connected to a single geodetic GNSS antenna and driven by an external UTC(PTB) frequency signal. The main goal of our investigations was to explore the current technical limits of GNSS frequency transfer with state-of-the-art GNSS equipment. For this, we analyzed the recorded carrier phase observations with our in-house GNSS software in a single-difference approach between two receivers each. In this very specific zero-baseline, common-clock measurement configuration, after fixing the phase ambiguities to integer values, the remaining signal theoretically only contains the relative hardware delays between the receivers. Averaging these single differences (SDs) across all satellites yields a time series that represents exactly that. This method was applied to three different GPS and two different ionosphere-free observation type combinations. The instability of each receiver link was assessed by means of Allan deviations derived from averaged SDs. The results show that links consisting of two receivers of the same type reach lower instability ranges faster than the combination of two different receiver types. One reason for this are the different tracking modes used by JAVAD and Septentrio receivers. In summary, the 10^{-18} instability range was only reached by the intra-receiver pairs, whereas the inter-receiver combination already hits its noise floor at $1.5 \cdot 10^{-17}$. Furthermore, the use of different observation type combinations only leads to small differences regarding the link instability.

Acknowledgements The authors would also like to thank Dr. Andreas Bauch and his team at PTB for their assistance and support in preparing, conducting and analyzing the experiment.

Conflict of Interest

The authors declare that they have no conflict of interest and that they do not attempt to recommend any of the instruments under test. It is noted that the performance of the equipment presented in this paper depends on the particular environment and the individual instruments in use. Other instruments of the same type or the same manufacturer may show different behavior. The readers are, however, encouraged to test their own equipment to identify the system performance with respect to a particular application.

References

Allan DW (1987) Time and frequency (time-domain) characterization, estimation, and prediction of precision clocks and oscillators. IEEE Trans Ultrason Ferroelectr Freq Control 34(6):647–654

Allan DW, Barnes JA (1981) A modified "Allan Variance" with increased oscillator characterization ability. In: Proceedings of the 35th annual frequency control symposium, Philadelphia, PA, USA, pp 470–475. https://doi.org/10.1109/FREQ.1981.200514

Bauch A, Weyers S, Piester D, Staliuniene E, Yang W (2012) Generation of UTC(PTB) as a fountain-clock based time scale. Metrologia 49(3):180–188. https://doi.org/10.1088/0026-1394/49/3/180

Defraigne P (2017) GNSS Time and frequency transfer. In: Teunissen PJG, Montenbruck O (eds) Springer handbook of global navigation satellite systems. Springer International Publishing, pp 1187–1206

JAVAD GNSS (2021) GNSS receiver TRIUMPH-OMEGA datasheet. https://download.javad.com/sheets/OMEGA_Datasheet.pdf

Katsigianni G, Loyer S, Perosanz F, Mercier F, Zajdel R, Sośnica K (2019) Improving Galileo orbit determination using zero-difference ambiguity fixing in a Multi-GNSS processing. Adv Space Res 63(9):2952–2963. https://doi.org/10.1016/j.asr.2018.08.035

Krawinkel T, Schön S, Bauch A (2021) Recent and future activities at Leibniz University Hannover in GNSS frequency transfer. In: 2021 joint conference of the European frequency and time forum and the IEEE international frequency control symposium

Loyer S, Perosanz F, Mercier F, Capdeville H, Marty JC (2012) Zero-difference GPS ambiguity resolution at CNES-CLS IGS Analysis Center. J Geodesy 86(11):991–1003. https://doi.org/10.1007/s00190-012-0559-2

Montenbruck O, Steigenberger P, Prange L, Deng Z, Zhao Q, Perosanz F, Romero I, Noll C, Stürze A, Weber G, Schmid R, MacLeod K, Schaer S (2017) The Multi-GNSS Experiment (MGEX) of the International GNSS Service (IGS) – Achievements, prospects and challenges. Adv Space Res 59(7):1671–1697. https://doi.org/10.1016/j.asr.2017.01.011

Petit G (2021) Sub-10^{-16} accuracy GNSS frequency transfer with IPPP. GPS Solutions 25(1). https://doi.org/10.1007/s10291-020-01062-2

Romero I (2020) RINEX: The Receiver Independent Exchange Format Version 3.05. https://files.igs.org/pub/data/format/rinex305.pdf

Weinbach U (2013) Feasibility and impact of receiver clock modeling in precise GPS data analysis: Dissertation. Veröffentlichungen der DGK Reihe C, Dissertationen, München: Verlag der Bayerischen Akademie der Wissenschaften. http://www.dgk.badw.de/fileadmin/user_upload/Files/DGK/docs/c-692.pdf

Weinbach U, Schön S, Feldmann T (2009) Evaluation of state-of-the-art geodetic GPS receivers for frequency comparisons. In: 2009 joint conference of the European frequency and time forum and the IEEE international frequency control symposium, pp 263–268. https://doi.org/10.1109/FREQ.2009.5168182

Zumberge JF, Heflin MB, Jefferson DC, Watkins MM, Webb FH (1997) Precise point positioning for the efficient and robust analysis of GPS data from large networks. J Geophys Res Solid Earth 102(B3):5005–5017. https://doi.org/10.1029/96JB03860